Research Article

Shah Hussain*, Hani S. H. Mohammed Ali, Shahid Ali Khan*, Aliya Farooq, Najla bint Saud Al-Saud, Yasir Anwar, Abdullah M. Asiri, Zia Ur Rahman, Noor ul Amin, and Sher Bahadar Khan*

Synthesis of biomass-supported CuNi zero-valent nanoparticles through wetness co-impregnation method for the removal of carcinogenic dyes and nitroarene

https://doi.org/10.1515/gps-2020-0028
received August 21, 2019; accepted February 04, 2020

Abstract: Stabilization of zero-valent CuNi nanoparticles (NPs) supported on *Cicer arietenum* (CP) is reported here for the reduction and removal of persistent organic pollutants. The functional groups and interactions of NPs with the CP were determined by ATR-FTIR. The crystallinity, morphology, and the elemental composition of the samples were determined through powder XRD, FESEM, and EDS techniques, respectively. The XRD spectrum displayed a sharp crystalline peak at 43.9 for CuNi. The Cu and Ni zero-valent NPs displayed a peak at almost the same region, and thus, both the peaks are merged and appeared as a single peak. The chemical reduction/degradation of eight model pollutants, viz., 2-nitrophenol (ONP), 3-nitrophenol (MNP), 4-nitrophenol (PNP), 2,4-dinitrophenol (DNP), methyl orange (MO), congo red (CR), methylene blue (MB), and rhodamine B (RB) were carried out in the presence of $NaBH_4$. The k_{app} value of 0.1 mM 4NP was highest which was 1.8×10^{-1} min^{-1} while the slowest rate was observed for CR and RB with k_{app} 5.5×10^{-3} and 5.4×10^{-3} min^{-1} respectively. This article helps in the removal of toxic organic pollutants through green supported NPs.

Keyword: biomass, CuNi, characterization, water treatment

*** Corresponding author: Shah Hussain,** Department of Chemistry, Abdul Wali Khan University, Mardan 23200, Pakistan; Department of Chemistry Government Postgraduate College, Nowshera-24100, Khyber-Pakhtunkhwa, Pakistan,
e-mail: shahhussain129@gmail.com
*** Corresponding author: Shahid Ali Khan,** Department of Chemistry, University of Swabi, Anbar-23561, Khyber Pakhtunkhwa, Pakistan; Center of Excellence for Advanced Materials Research (CEAMR), King Abdulaziz University, P. O. Box 80203, Jeddah, 21589, Saudi Arabia; Department of Chemistry, King Abdulaziz University, P. O. Box 80203, Jeddah, 21589, Saudi Arabia,
e-mail: sbkhan@kau.edu.sa
*** Corresponding author: Sher Bahadar Khan,** Center of Excellence for Advanced Materials Research (CEAMR), King Abdulaziz University, P. O. Box 80203, Jeddah, 21589, Saudi Arabia; Department of Chemistry, King Abdulaziz University, P. O. Box 80203, Jeddah, 21589, Saudi Arabia,
e-mail: shahidsawal007@gmail.com
Hani S. H. Mohammed Ali: Department of Biological Sciences, Faculty of Science, King Abdulaziz University, P. O. Box 80203, Jeddah, 21589, Saudi Arabia
Aliya Farooq: Department of Chemistry, Shaheed Benazir Bhutto Women University, Peshawar, Pakistan
Najla bint Saud Al-Saud: Princess Najla bint Saud Al-Saud Center for Excellence Research in Biotechnology, King Abdulaziz University, Jeddah, Saudi Arabia
Yasir Anwar: Department of Biological Sciences, Faculty of Science, King Abdulaziz University, P. O. Box 80203, Jeddah, 21589, Saudi Arabia
Abdullah M. Asiri: Center of Excellence for Advanced Materials Research (CEAMR), King Abdulaziz University, P. O. Box 80203, Jeddah, 21589, Saudi Arabia; Department of Chemistry, King Abdulaziz University, P. O. Box 80203, Jeddah, 21589, Saudi Arabia
Zia Ur Rahman: Department of Chemistry, University of Swabi, Anbar-23561, Khyber Pakhtunkhwa, Pakistan
Noor ul Amin: Department of Chemistry, Abdul Wali Khan University, Mardan 23200, Pakistan

1 Introduction

The zero-valent metal NPs are much more reactive than their bulk materials due to their high Fermi potential resonance and small quantum size effects. These characteristics of the zero-valent metal NPs make them one of the most versatile materials in the field of catalysis [1]. Zero-valent metal NPs have a large surface-to-volume ratio. This high surface area provides new and novel features to these materials. The field of zero-valent metal NPs is the emerging research at the industrial level as it is used in the field of catalysis, photocatalysis, biological sectors, water splitting, sensors, and many others [1–8]. Literature has reported many methods for the synthesis of zero-valent metal NPs including chemical, physical, and biological. Chemical fabrication involves organic solvents and other

reducing agents to support and stabilize the NPs, but it is not eco-friendly [6]. Physical methods involve thermal evaporate, plasma arcing, pulsed laser, ball milling, ultra-thin films, spray pyrolysis, lithographic techniques, desorption, diffusion flame, sputter deposition, and molecular beam epistaxis [3]. Chemical methods involve electrode position, sol–gel process, chemical vapor deposition, chemical solution deposition, Langmuir–Blodgett method, soft-chemical method, hydrolysis, catalytic route, wet-chemical method, and co-precipitation [3,9]. However, excessive chemical use, radiation, and nonecofriendly methods limit the use of these practices [10–12]. Therefore, a more reliable, cost-effective, and eco-friendly procedure is required [4,13–16]. Plant and plant-derivative materials are suitable candidates for such processes. Plant materials with their secondary metabolites are responsible for the support and stabilization of NPs [17,18]. In this article, the *Cicer arietinum* was used for the stabilization of CuNi NPs. The *C. arietinum* is a legume of the family Fabaceae and subfamily Faboideae and is largely used for making different foodstuffs. In South Asia, Bengal grams and chickpeas are used to make curry, which is one of the most popular vegetarian food served with steamed rice and bread in the Diaspora community of various countries [16]. In Indian cuisine, popular dishes are made with chickpeas flour such as mirapakaya mirchi bada. The unripe chickpeas leaves are eaten as food vegetable salad and as a raw snack [12]. The *C. arietinum*-supported CuNi NPs can be applied for the removal of toxic organic pollutants from the effluents. Nitrophenols and dyes are organic pollutants that have detrimental effects on human health and other living organisms; hence, their removal is inevitable [17]. The toxicity of nitrophenols is adverse to such an extent that various nitrophenols have been listed as "Priority Pollutant" by the U.S. Environmental Protection Agency and strict laws have been framed to control the release of these hazardous chemicals into the natural waters (U.S. EPA, 1976). Principles have been made, and strict constraints are imposed on the industries to control the release of these pollutants into the environment (U.S. EPA, 1988) [18–20]. The removal of these pollutants is of utmost importance due to their large scale use in the agriculture and industrial sectors [18–22]. From both sectors, excess concentration of these pollutants find their way into the water resources and thus contaminate the natural water bodies. Nitrophenols have some disturbing effects on liver, kidney, stomach, and central nervous system [19,23]. Dyes are the other pollutants, which is a matter of serious concern at the global level because even the presence of meagre concentration in water makes it colorful. The presence of unwanted color reduces the penetration of air, oxygen, and sunlight into the water bodies, which has a detrimental effect on the aquatic flora and fauna. Approximately, 10,000 dyes are commercially available and are largely used in the textile, paper, hides, and skin industries, which are also used for other coloring purposes [24]. Unfortunately, it is easier for industries to release their waste materials in the surroundings rather than treatment [25,26]. The removal of these unwanted chemicals and dyes is the pressing need of time [27]. In this research work, an attempt has been made on the zero-valent metal NPs, which is one of the most emerging research for the removal of hazardous chemicals from the effluents [28–30]. The use of CP powder for the stabilization of CuNi NPs has not yet been reported, and to the best of authors' knowledge, no publications have been reported yet.

2 Experimental

2.1 Materials

2-Nitrophenol (ONP), metanitrophenol (MNP), para nitrophenol (PNP), 2,4-dinitrophenol (DNP), congo red (CR), methyl orange (MO), and rhodamine B (RB) were purchased from Sigma Aldrich. The methylene blue dye (MB), reducing agent $NaBH_4$, $CuSO_2$, and $NiCl_2$ were obtained from Daejung Chemicals, South Korea, Germany. *C. arietinum* was purchased from the local market.

2.2 Preparation of CuNi NPs

First, CP fine powder was obtained by blending CP with the help of an electric blender for about 20 min. Afterward, 1 g of this powder was added to a 100 mL solution comprising 50 mL of 0.2 M solution of $NiCl_2{\cdot}6H_2O$ and 50 mL of 0.2 M solution of $CuSO_4{\cdot}5H_2O$. For complete saturation of the adsorptive sites on CP, the powder was allowed to stir in the solution for 6 h. After the adsorption of the salts, the color of the CP changed, which is indicative of the metal salts adsorption. The CP adsorbed metal salts were collected and washed several times with double distilled water to remove any nonadsorbed metal salts. It was then dried at normal temperature and stored in clean tubes. The CP-adsorbed CuNi ions were treated

with X mL of 1 M $NaBH_4$ solution, which turned the Cu^{2+} and Ni^{2+} ions into CuNi zero-valent NPs, which turned the color of the sample black. The appearance of black color is the first indication of the formation of CuNi zero-valent NPs. The synthesized CuNi NPs were then used for the reduction of nitro groups in nitrophenols and discoloration of various dyes in the presence of $NaBH_4$.

2.3 Catalytic reduction/removal reactions

For the reduction/removal of all the pollutants, 2.5 mL of each pollutant was treated with 0.5 mL of $NaBH_4$ and 10 mg of the NPs and then the rate of reduction/removal and degradation of the pollutants was monitored in a time-dependent UV-Vis spectrophotometer.

The following formula (equation (1)) was used for the decrease in the original concentration of the pollutants:

$$\frac{C_t}{C_0} \tag{1}$$

Equation (1) indicated the final concentration (C_t) and initial concentration (C_0) of the targeted pollutants.

The percent reduction/removal of all the pollutants as a function of contact time was deduced from the following formula (equation (2)):

$$\frac{A_0 - A_t}{A_0} \times 100 \tag{2}$$

In equation (1), A_t is the final absorbance of the pollutant and A_0 is the initial absorbance of the model pollutants.

While the k_{app} value of the reduction and degradation of nitrophenols and dyes were inferred from the first-order kinetics presented in equation (3) as follows:

$$\ln \frac{C_t}{C_0} \tag{3}$$

where ln is the natural logarithm and C_t and C_0 indicate the final and initial concentrations of the documented pollutants.

2.4 Instrumental characterization

The sharp fine crystalline peaks of the CuNi NPs were obtained through powdered XRD spectrum (Thermo scientific diffractometer) of Cu Kα radiations having λ = 0.154 nm from 2θ = 10–80°. Morphology (shape and particle size) of NPs were resolute by Field Emission-Scanning Electron Microscope (FESEM) JEOL (JSM-7600F, Japan). Similarly, the functional group analysis in both plant and NPs were observed by ATR-FTIR spectroscopy (Nicolet 50 ATR-FTIR spectrometer Thermo Scientific). The batch experiment for the reduction and degradation of all the pollutants was done through a UV-visible spectrophotometer (Shimadzu, MultiSpec1501).

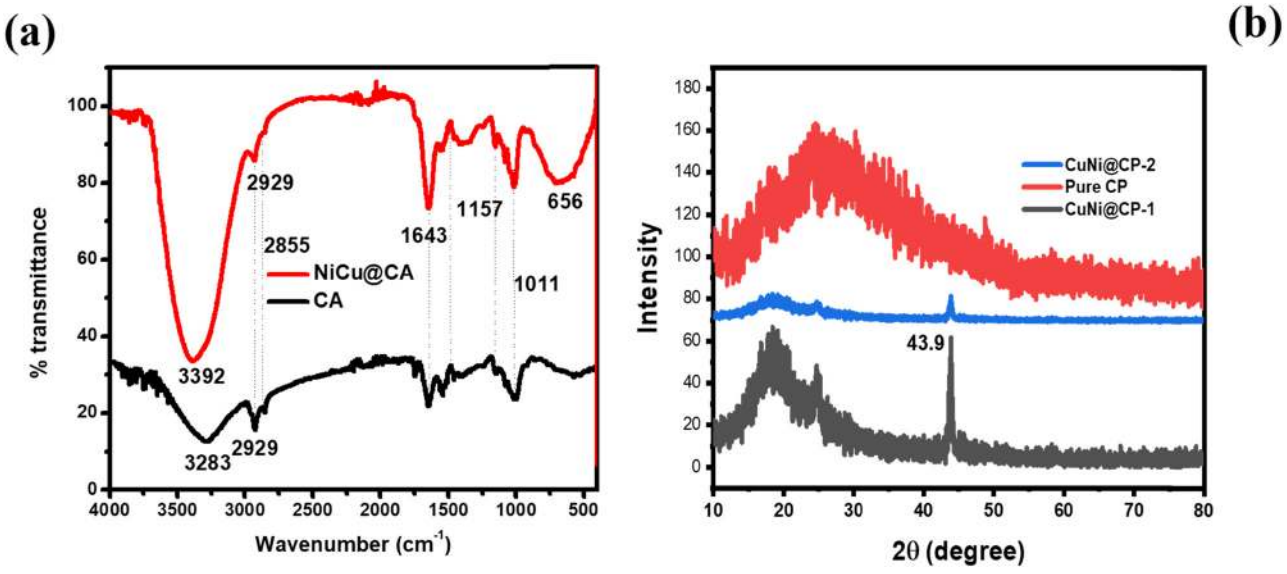

Figure 1: FTIR (a) and XRD (b) spectrum of CP and CuNi@CP NPs. In the XRD spectrum, CuNi@CA-1 and CuNi@CA-2 indicated the XRD spectrum before and after the reactions, respectively.

3 Results and discussion

The FTIR spectrum was recorded from 500 to 4,000 cm^{-1} range as shown in Figure 1a. A sharp intense peak appeared at 3,392 cm^{-1} for –OH stretching vibration. The sharpness of the peak suggested the multiple H-bonding in the CuNi@CP NPs. However, a less intense peak for –OH which appeared at 3,283 cm^{-1} was also observed for the pure CP. The difference in both peaks might be due to the involvement of H-bonding in the NPs formation. The absorption at 1,643 cm^{-1} reflects the bending vibration mode of –OH. Other important peaks at 2,929 and 2,855 cm^{-1} were due to the C–H stretching vibrations. Other noticeable peaks in the NPs and pure CP were observed at 1157, 1011 cm^{-1} due to C–O bending vibration. M–O bond in the NPs appeared at 656 cm^{-1} [19,25].

The XRPD spectrum indicated a broad hump at 2θ = 26.2° for the pure CP, confirming the amorphous nature of CP. However, after stabilizing the CuNi NPs with the help of CP, a sharp peak at 2θ = 43.9° indicated the crystalline nature of CuNi, while the peak at 2θ = 24.7° is due to the metal oxide [6]. Along with the crystalline peaks, a hump at 2θ = 18.5° appeared for the amorphous

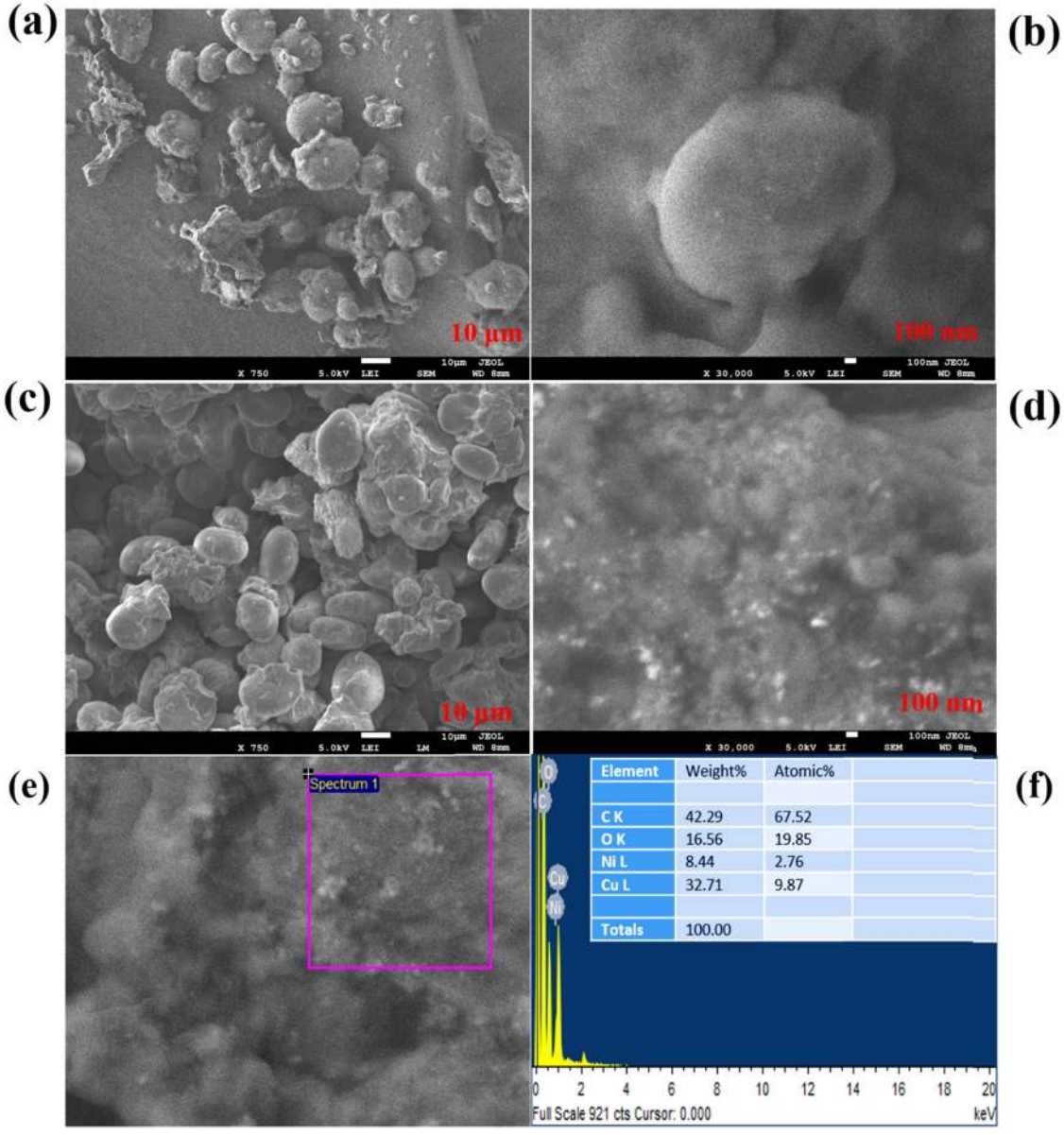

Figure 2: FESEM images of pure CP (a and b) and Ni-CP nanoparticles (c and d), the left side images are at low resolutions (10 µm), while the right side images are at high resolution (100 nm). Area selection for EDS spectrogram (e) and elemental analysis window (f) of CuNi@CP NPs.

nature of CP. The stong interaction of NPs with the CP has shifted the amorphous peak of the CP as depicted in Figure 1b. The XRD analysis was carried out after three-run, and it was observed that the intensity of the peak was decreased possibly the leaching of the NPs.

The FESEM was carried out for the surface morphology of the CuNi NPs. The low- and high-resolution images are indicated on the left and right sides of Figure 2a and d, respectively. The low resolution was carried out at 10 µm and high at 100 nm, respectively. The low resolution of pure CP not showing any NPs; at high resolution, the pure CP does not show any NPs. However, CuNi@CP indicated the presence of NPs. The high-resolution FESEM images of CuNi@CP indicated a bright spot of NPs, which suggested that NPs are strongly interacting with the chemical constituents of CP.

EDS spectrum indicating the purity of the sample and used for the elemental analysis of the prepared sample (Figure 2e and f). The EDS displayed peaks for C, O, Cu, and Ni elements. The C and O appeared in 42.29 and 16.56 by weight%, while the Ni and Cu are 8.44 and 32.71 by weight%. The C, O, Ni, and Cu are displayed at 0.2, 0.5, 0.9, and 1.1 keV.

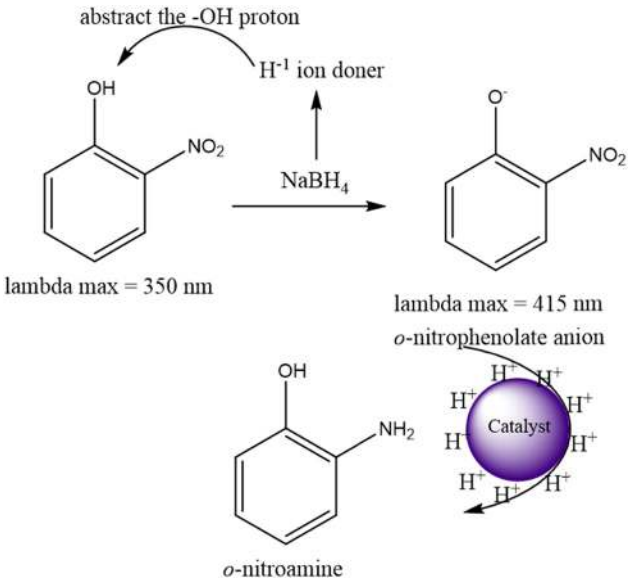

Scheme 1: Pictorial representation for the reduction of ONP in the presence of $NaBH_4$ as a reductant and CuNi@CP NPs.

3.1 Reduction of isomeric nitrophenols

Nitrophenols are extremely toxic organic compounds and are ranked among the most hazardous pollutants. According to the U.S. Environmental Protection Agency, the PNP, ONP, and 2,4-dinitrophenol are the most dangerous pollutants and listed as "Priority Pollutants." Environmental protection agency is up for implementing strict restrictions to control the concentrations of these hazardous pollutants in natural waters to <10 ng/L (U.S. EPA, 1976). Nitro group-containing compounds are distressing to liver, kidney, and central nervous system of living organism especially human beings. Therefore, careful and robust technology is the need of time to eradicate these pollutants from the wastewater. For this reason, CuNi@CP NPs were developed for the reduction of isomeric ONP, MNP, and PNP as well as DNP to the amino group.

Initially, the ONP is treated without the CuNi@CP NPs, with which no change was observed in the absorbance. After that, $NaBH_4$ redshift has been observed in the λ_{max} of ONP and has been shifted from 350 to 415 nm. $NaBH_4$ abstract the proton from the –OH group of ONP which results in the formation of the *o*-nitrophenolate anion. It is well known that the negative charge becomes more stable on the most electronegative atom; therefore, the negative charge on the oxygen becomes more stable and delocalized more as compared with the lone pair electrons on –OH group. Furthermore, delocalization weekens the bonds and increases the bond length, that is why after the addition of $NaBH_4$, redshift has been observed in the UV-Vis spectrum of ONP.

Table 1: Comparison of the data with the literature for the reduction of PNP

Catalyst	Targeted materials	Concentration of the targeted pollutant ppm	Amount of the catalyst (mg/mL)	Reaction time	References
Chitosan@Ag	Para	14.00	0.4	30.00	[31]
Ni_2S_3@C	nitrophenol (PNP)	20.00	5.00	48.33	[11]
(G8)-AgNi		41.96	0.10	38.00	[32]
PS@PAMAM		15.00	0.10	60.00	[33]
CuNi@CP		14	2.50	7.00	This work

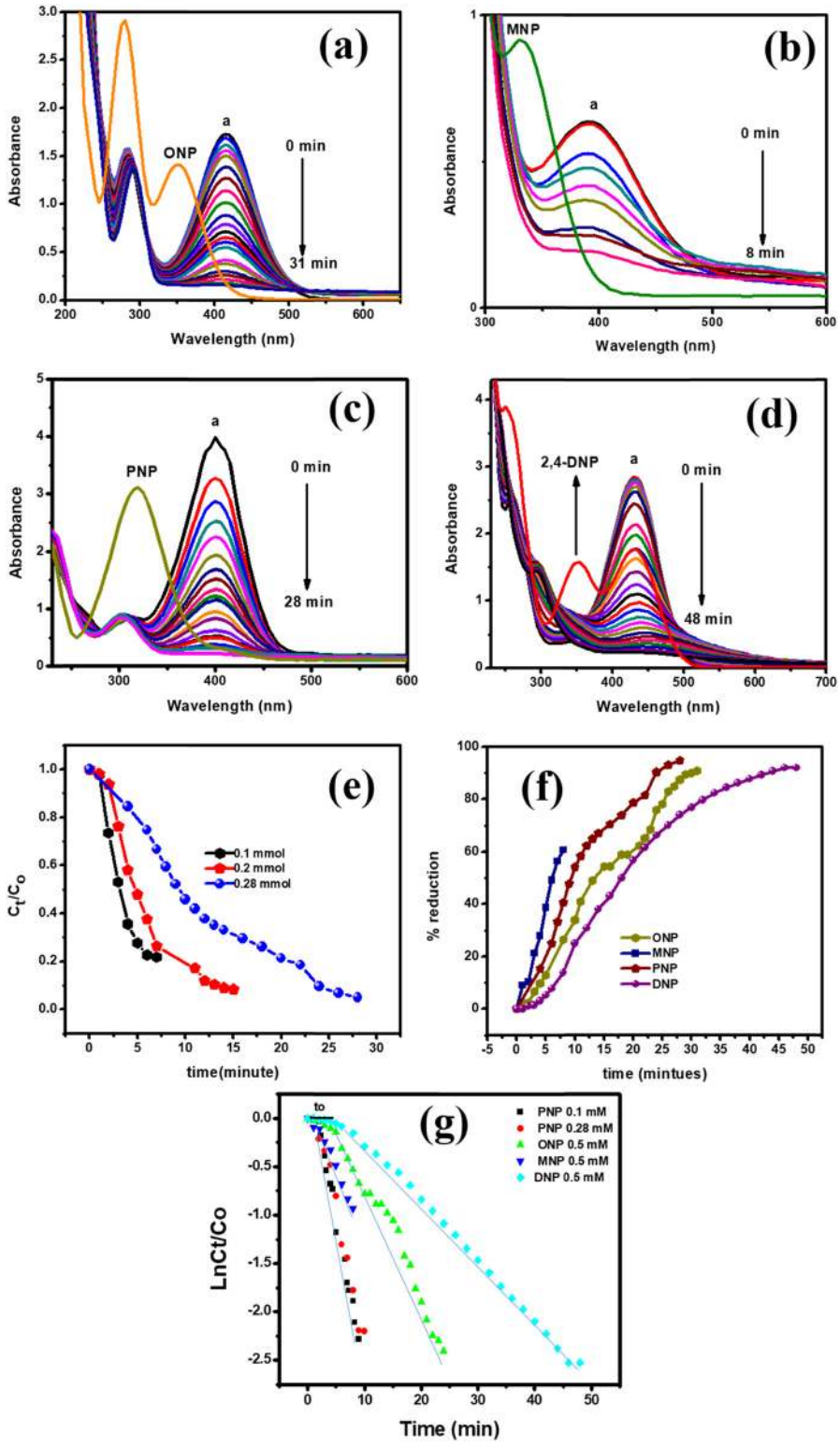

Figure 3: Time-dependent UV-Vis spectrum for the reduction of ONP (a), MNP (b), PNP (c), and DNP (d), the labeled a in the spectrum (a–d) showing the phenolate ion, which is formed after the addition of $NaBH_4$, while the pure nitrophenol is designated by their name in the spectrum (a–d), kinetic data C_t/C_0 for the different concentration of PNP (0.1, 0.2 and 0.28 mM) (e) and % reduction of all nitrophenols (f). ONP, MNP, and DNP are 0.5 mM while the PNP in the % reduction graph is 0.28 mM, the k_{app} value and R^2 value deduced from the linear equation ln C_t/C_0 (g).

Furthermore, the reduction of nitrophenols to aminophenol with $NaBH_4$ as a reducing agent is a thermodynamically favorable reaction, but kinetically unfavorable reaction. Therefore, an efficient and effective catalyst is required for this reduction reaction. In the next stage, 10 mg of the CuNi@CP NPs was introduced to the ONP solution along with the $NaBH_4$ in the UV cuvette to make this reduction reaction kinetically favorable by minimizing the activation energy barrier. The reduction of ONP in the presence of $NaBH_4$ and catalyst is diagrammatically represented in Scheme 1. The data of PNP are compared with the data reported in the literature as depicted in Table 1.

A 2.5 mL of 0.5 mM of a solution of all the ONP, MNP, and DNP were treated against 10 mg of the CuNi@CP NPs and monitored the reduction of nitrophenols to aminophenol in the time-dependent UV-Vis spectrophotometer. The concentration of PNP was 0.28 mM because the high concentration of PNP is going out of the UV-Vis range.

The λ_{max} of ONP, MNP, PNP, and DNP was ~350, ~290, ~318,0 and ~350 nm; however, after reaction with $NaBH_4$, ONP, MNP, PNP, and DNP, the corresponding λ_{max} changed to 415, 328, 400, and 430 nm, and all these nitrophenols turned pale to sharp yellow color. The decrease in the concentration of various nitrophenols with contact time is represented in Figure 3a–d. The reason for their redshift was due to their extended conjugation. The explanation is that when negative charge resides on the most electronegative atom, it is more stabilized that is why the lone pair of –OH not so delocalized as compared to their corresponding anions.

The CuNi@CP (10 mg) catalyst is used for the reduction of 3 mL of 0.5 mM solution of ONP, MNP, and DNP while the same amount of the catalyst was used against 0.28 mM of 2.5 mL solution of PNP. To each solution, 0.5 mL of 1 mM aqueous $NaBH_4$ was added. With the addition of $NaBH_4$, redshift was observed in all the nitrophenols. The decrease in the concentration of ONP, MNP, PNP, and DNP was monitored at λ_{max} 415, 328, 400, and 430 nm as a function of contact time. The change in the original concentration was deduced from equation (1).

The % reduction of the ONP, MNP, PNP, and DNP indicated a continuous increase in reaction progress. All the pollutants were allowed to reduced till 100% or close to 100% and then the time was noted. It was observed that 90.99% of ONP is reduced to *o*-aminophenol in 31 min, 94.91% of 0.28 mM of PNP is reduced to *p*-aminophenol in 28 min, and 92.0% of DNP is reduced to di-aminophenol in 48 min. However, only 60.7% of MNP is reduced in 8 min, and no further reduction was observed as it became constant shown in Figure 3f.

The rate of reaction of different nitrophenols was determined from $\ln C_t/C_0$.

3.2 Effect of PNP concentration

The effect of concentration of the pollutants was checked against the CuNi@CP NPs, different concentrations such as 0.28, 0.2 and 0.1 mM of PNP were selected and to each one, 10 mg of CuNi@CP NPs was added in all the experiments. It was observed that the rate of reaction increased with the decrease in the PNP concentration from 0.28 to 0.1 mM. The 0.28 mM PNP was reduced to *p*-aminophenol in 28 min, 0.2 mM in 15 min, and 0.1 mM in 7 min. This reflects that by increasing the concentration of analyte, the active sites of the catalyst saturate sooner as compared with the low concentration of the analyte (Figure 3e). The $\ln C_t/C_0$ indicating the highest reduction rpm for 0.1 mM PNP, which is 1.8×10^{-1} min^{-1} while the R^2 value is 0.91449 (Figure 3g). Similarly, the k_{app} and R^2 values for other nitrophenols are presented in Table 2.

3.3 Discolorization of dyes

The degradation of two anionic and two cationic dyes was considered in this experiment. The anionic dyes were CR and MO, and the cationic dyes were MB and RB. The same protocol was followed as discussed for the nitrophenols. Three milliliters of 0.05 mM of all the dyes was taken in a quartz cuvette with the addition of 0.5 mL of 1 mM $NaBH_4$ solution. Like nitrophenols, the $NaBH_4$

Table 2: The k_{app} and R^2 values the pollutant were derived from the first-order kinetic $\ln C_t/C_0$

Pollutant	k_{app} (min^{-1})	R^2
PNP (0.1 mM)	1.8×10^{-1}	0.91449
PNP (0.2 mM)	1.6×10^{-1}	0.88977
PNP (0.28 mM)	1.3×10^{-1}	0.89976
ONP	7.2×10^{-2}	0.96187
MNP	4.7×10^{-2}	0.98594
DNP	6.3×10^{-2}	0.94728
CR	5.5×10^{-3}	0.979
MO	9.3×10^{-1}	0.9926
MB	2.59×10^{-2}	0.8913
RB	5.4×10^{-3}	0.963

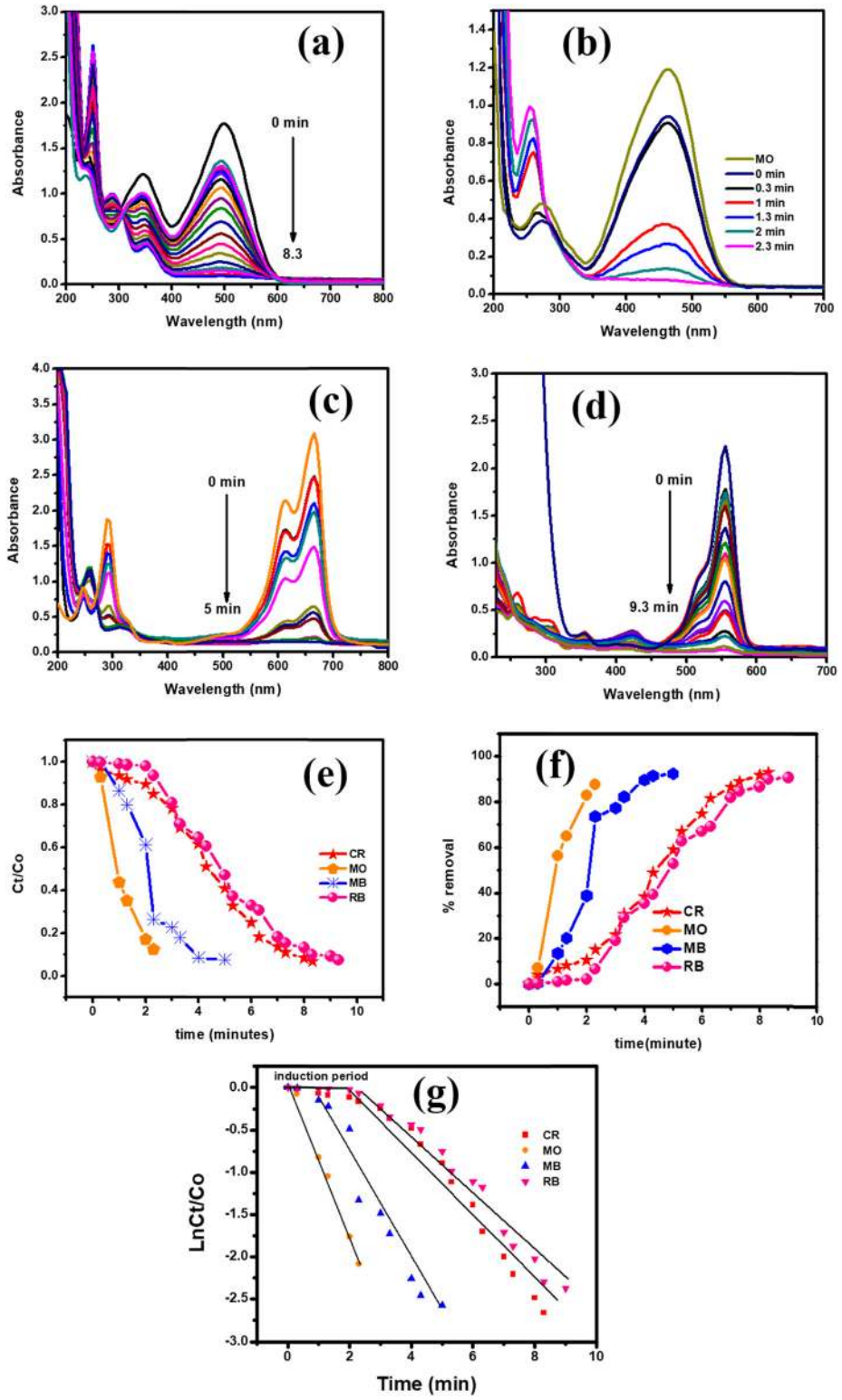

Figure 4: Time-dependent UV-Vis spectrum for the degradation of CR (a), MO (b), MB (c), and RB (d), the concentration of all the dyes are 0.05 mM and 0.5 mL of 1 M $NaBH_4$ and 10 mg of the CuNi@CP catalyst was used in this experiment. The kinetic data C_t/C_0 (e) and % removal (f) showing the strongest activity of MO dye, the k_{app} and R^2 value determined from the trendline of ln C_t/C_0 (g).

alone does not degrade the dyes, it is the catalyst that actually takes over the activation energy barrier and makes this reaction kinetically feasible. $NaBH_4$ changed the azo groups of MO and CR dyes to their hydrazine form and MB and RB dyes to their luco MB and luco RB form as shown in the inset of Figure 4. The λ_{max} of CR, MO, MB, and RB before and after the addition of $NaBH_4$ appeared at 500, 465, 665, and 454 nm, respectively. After the addition of 10 mg of the catalyst to their respective solution, the absorbance of each dye decreased as a function of time. It was observed that CR degraded in 8.3 min (Figure 4a), MO in 2.3 min (Figure 4b), MB in 5 min (Figure 4c), and RB in 9 min (Figure 4d). The decrease in the original concentration of the dyes, the percent removal of all the dyes, and the rate of reaction were deduced from equations (1)–(3), respectively. The C_t/C_0 suggested the decrease in the concentration in the order as MO > MB > CR > RB (Figure 4e), while the percent degradation indicated 92.99% removal of CR in 8 min, 87.5% of MO in 2.3 min, 92.4% of MB in 5 min, and 90.6% of RB in 9 min (Figure 4f). The rate of reaction was determined from the first-order kinetics and presented in Table 2. The k_{app} and R^2 values of all the dyes were determined from the $\ln C_t/C_0$ as indicated in the inset of Figure 4g.

3.4 Mixed system

The catalytic activity of the CuNi@CP NPs was checked against the simultaneous removal of PNP, CR, and MB dyes to check the selectivity of the reaction. The mixed system is extremely important in case where the simultaneous degradation of pollutants is required. Three different attempts were made for the simultaneous removal of PNP and dyes. In the first attempt, PNP–CR (Figure 5a) are removed, and in the second attempt, PNP–MB are removed (Figure 5b), and in the third attempt, PNP–CR–MB are removed (Figure 5c). No chemical reactions were observed after mixing the respective dyes with PNP and $NaBH_4$. The UV-Vis spectrum indicated two λ_{max} for PNP–CR at 400 and 500 nm and PNP–MB at 400 and 670 nm, and three λ_{max} appeared for the PNP–CR–MB system at

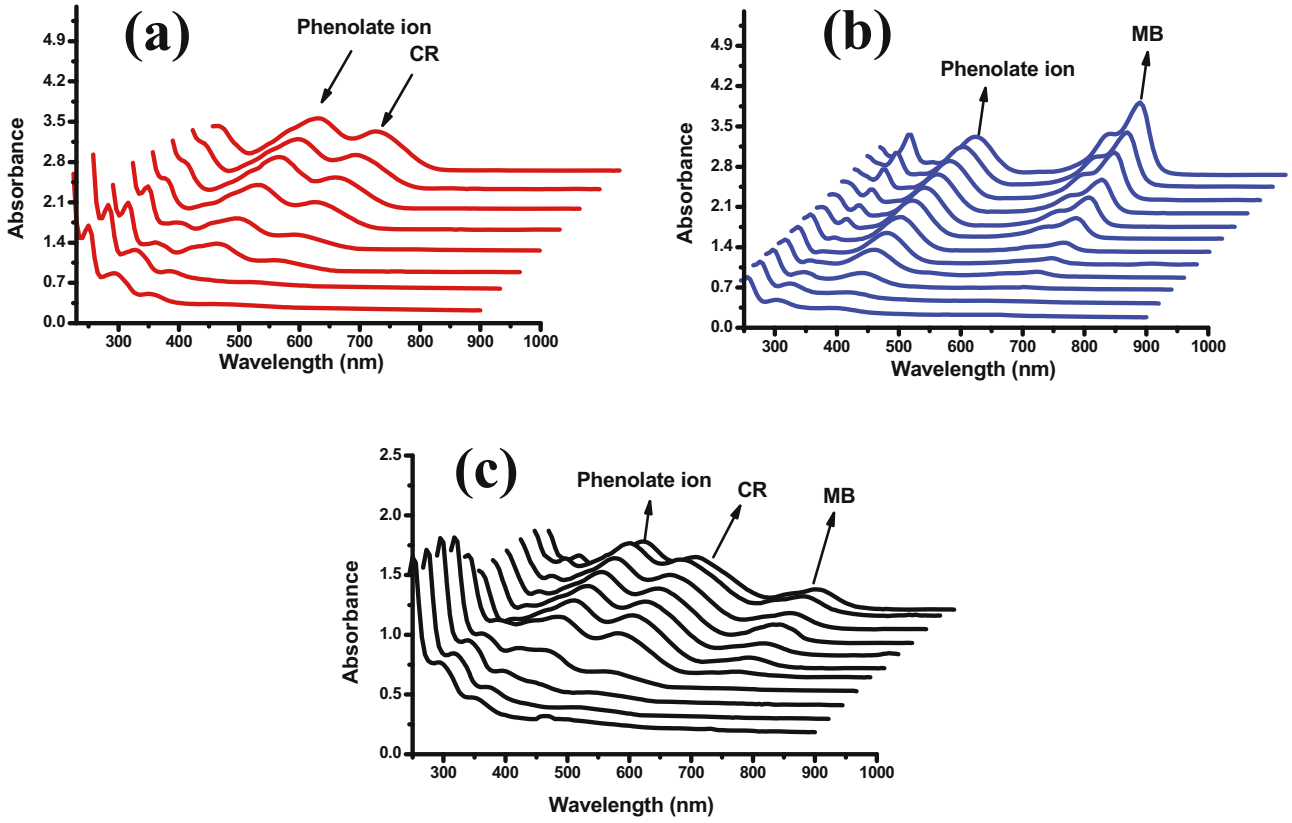

Figure 5: Time-dependent UV-Vis spectrum for the removal of a mixed system of dyes and PNP (a) represent the mixed system of CR-PNP degraded in 6 min, (b) MB-PNP degraded in 10 min, and (c) MB-PNP-CR degraded in 9 min. The results show the selectivity of MB as compared to CR and PNP.

400, 500, and 760 nm. These λ_{max} values indicated that dyes and nitrophenol remained mixed up without any chemical reaction.

Three milliliters of 0.05 mM CR and 3 mL of 0.1 mM PNP solution was mixed in a clean vial, to this solution 1 mL of 1 mM NaBH4 solution was added. From this solution, 3 mL of the solution in a quartz cuvette was taken and 10 mg of the catalyst was added. Figure 5a clearly indicates that CR degraded first as compared to PNP; however, after 6 min, the whole solution degraded. The similar experimental protocol was followed for PNP–MB and PNP–CR–MB, where MB is degraded before PNP (Figure 5b), and PNP and CR (Figure 5c), respectively. This shows that MB is selective over both CR and PNP and CR is selective over PNP.

4 Conclusion

The CuNi NPs were supported on the *C. arietinum* and were used for the removal of nitrophenols and organic dyes. The rate of reaction was determined through first-order kinetics, and among all the nitrophenols, the removal rate was highest for ONP followed by ONP, DNP, and MNP, respectively. The highest rate of removal was recorded for MO followed by MB and RB and CR. The synthesized NPs were also applied for the simultaneous removal of nitrophenols and dyes.

Acknowledgment: The authors highly acknowledge AWKUM, CEAMR, department of chemistry KAU in collaboration with the Department of Chemistry University of Swabi, Pakistan.

Conflict of interest: The authors confirm no conflict of interest.

References

[1] Albanese A, Tang PS, Chan WC. The effect of nanoparticle size, shape, and surface chemistry on biological systems. Annu Rev Biomed Eng. 2012;14:1–16.

[2] Baran T, Mahmoud N. Facile synthesis of palladium nanoparticles immobilized on magnetic biodegradable microcapsules used as effective and recyclable catalyst in Suzuki–Miyaura reaction and *p*-nitrophenol reduction. Carbohydr Polym. 2019;222:115029.

[3] Bello BA, Khan SA, Khan JA, Syed FQ, Anwar Y, Khan SB. Antiproliferation and antibacterial effect of biosynthesized AgNps from leaves extract of Guiera senegalensis and its catalytic reduction on some persistent organic pollutants. J Photochem Photobiol B: Biol 2017;175:99–108.

[4] Bello BA, Khan SA, Khan JA, Syed FQ, Mirza MB, Shah L, et al. Anticancer, antibacterial and pollutant degradation potential of silver nanoparticles from Hyphaene thebaica. Biochem Biophys Res commun. 2017;490(3):889–94.

[5] Chen Z, Leng K, Zhao X, Malkhandi S, Tang W, Tian B, et al. Interface confined hydrogen evolution reaction in zero valent metal nanoparticles-intercalated molybdenum disulfide. Nat Commun. 2017;8:14548.

[6] Darband GB, Aliofkhazraei M, Rouhaghdam AS. Nickel nanocones as efficient and stable catalyst for electrochemical hydrogen evolution reaction. Int J Hydrog Energy. 2017;42(21):14560–5.

[7] Devaraj M, Saravanan R, Deivasigamani R, Gupta VK, Gracia F, Jayadevan S. Fabrication of novel shape Cu and Cu/Cu_2O nanoparticles modified electrode for the determination of dopamine and paracetamol. J Mol Liq. 2016;221:930–41.

[8] Erci F, Cakir-Koc R, Isildak I. Green synthesis of silver nanoparticles using Thymbra spicata L. var. spicata (zahter) aqueous leaf extract and evaluation of their morphology-dependent antibacterial and cytotoxic activity. Artif Cell Nanomed biotechnol. 2018;46:150–8.

[9] Erci F, Cakir-Koc R, Isildak I. Green synthesis of silver nanoparticles using Thymbra spicata L. var. spicata (zahter) aqueous leaf extract and evaluation of their morphology-dependent antibacterial and cytotoxic activity. Artif Cell Nanomed Biotechnol. 2018;46:150–8.

[10] Foxx D, Kalu EE. Amperometric biosensor based on thermally activated polymer-stabilized metal nanoparticles. Electrochem Commun. 2007;9(4):584–90.

[11] Gao L, Li R, Sui X, Li R, Chen C, Chen Q. Conversion of chicken feather waste to N-doped carbon nanotubes for the catalytic reduction of 4-nitrophenol. Env Sci Technol. 2014;48(17):10191–7.

[12] Gaur Y, Sen A. Cross inoculation group specificity in Cicer-rhizobium symbiosis. N Phytologist. 1979;83(3):745–54.

[13] Gul S, Rehan ZA, Khan SA, Akhtar K, Khan MA, Khan M, et al. Antibacterial PES-CA-Ag_2O nanocomposite supported Cu nanoparticles membrane toward ultrafiltration. BSA Rejection Reduct Nitrophenol J Mol Liq. 2017;230:616–24.

[14] Gupta VK, Nayak A, Agarwal S, Tyagi I. Potential of activated carbon from waste rubber tire for the adsorption of phenolics: effect of pre-treatment conditions. J Colloid Interf Sci. 2014;417:420–30.

[15] Islam MT, Dominguez N, Ahsan MA, Dominguez-Cisneros H, Zuniga P, Alvarez PJ, et al. Sodium rhodizonate induced formation of gold nanoparticles supported on cellulose fibers for catalytic reduction of 4-nitrophenol and organic dyes. J Env Chem Eng. 2017;5(5):4185–93.

[16] Jain M, Misra G, Patel RK, Priya P, Jhanwar S, Khan AW, et al. A draft genome sequence of the pulse crop chickpea (Cicer arietinum L.). Plant J. 2013;74(5):715–29.

[17] Kamal T, Khan SB, Asiri AM. Nickel nanoparticles-chitosan composite coated cellulose filter paper: an efficient and easily recoverable dip-catalyst for pollutants degradation. Env Pol. 2016;218:625–33.

[18] Kamal T, Khan SB, Asiri AM. Synthesis of zero-valent Cu nanoparticles in the chitosan coating layer on cellulose

microfibers: evaluation of azo dyes catalytic reduction. Cellulose. 2016;23(3):1911–23.
[19] (a)Khan SA, Bello BA, Khan JA, Anwar Y, Mirza MB, Qadri F, et al. Albizia chevalier based Ag nanoparticles: anti-proliferation, bactericidal and pollutants degradation performance. J Photochem Photobiol B Biol. 2018;182:62–70; (b) Khan SA, Khan SB, Akhtar K, Farooq A. Nano-catalyst and nano-catalysis: state of the arts and prospects. Nanomaterials Environ Appl their Fascinating Attributes. 2018;2:290.
[20] Khan SA, Khan SB, Asiri AM. Toward the design of Zn–Al and Zn–Cr LDH wrapped in activated carbon for the solar assisted de-coloration of organic dyes. RSC Adv. 2016;6(86):83196–208.
[21] Khan SA, Khan SB, Farooq A, Asiri AM. A facile synthesis of CuAg nanoparticles on highly porous ZnO/carbon black-cellulose acetate sheets for nitroarene and azo dyes reduction/degradation. Intern J Biol Macromol. 2019;130:288–99.
[22] Khan SA, Khan SB, Kamal T, Yasir M, Asiri AM. Antibacterial nanocomposites based on chitosan/Co-MCM as a selective and efficient adsorbent for organic dyes. Intern J Biol Macromol. 2016;91:744–51.
[23] Khan SA, Khan SB, Khan LU, Farooq A, Akhtar K, Asiri AM. Fourier transform infrared spectroscopy: fundamentals and application in functional groups and nanomaterials characterization. In Handbook of Materials Characterization. Sharma SK, editor. Cham: Springer International Publishing; 2018. pp. 317–44.
[24] Sohni S, Khan SA, Akhtar K, Khan SB, Asiri AM, Hashim R, et al. Room temperature preparation of lignocellulosic biomass supported heterostructure (Cu + Co@OPF) as highly efficient multifunctional nanocatalyst using wetness co-impregnation. Colloids Surf A: Physicochem Eng Asp. 2018;549:184–95.
[25] Nasrollahzadeh M, Akbari R, Issaabadi Z, Sajadi SM. Biosynthesis and characterization of Ag/MgO nanocomposite and its catalytic performance in the rapid treatment of environmental contaminants. Ceram Intern. 2020;146(2):2093–101.
[26] Nasrollahzadeh M, Sajadi SM, Maham M, Kohsari I. Biosynthesis, characterization and catalytic activity of the Pd/bentonite nanocomposite for base-and ligand-free oxidative hydroxylation of phenylboronic acid and reduction of chromium(VI) and nitro compounds. Microporous Mesoporous Mater. 2018;15(271):128–37.
[27] Pakzad K, Alinezhad H, Nasrollahzadeh M. Green synthesis of Ni@Fe_3O_4 and CuO nanoparticles using Euphorbia maculata extract as photocatalysts for the degradation of organic pollutants under UV-irradiation. Ceram Intern. 2019;45(14):17173–82.
[28] Saleh TA, Gupta VK. Processing methods, characteristics and adsorption behavior of tire derived carbons: a review. Adv Colloid Interface Sci. 2014;1(211):93–101.
[29] Saleh TA, Gupta VK. Photo-catalyzed degradation of hazardous dye methyl orange by use of a composite catalyst consisting of multi-walled carbon nanotubes and titanium dioxide. J Colloid Interface Sci. 2012;371(1):101–6.
[30] Saravanan R, Sacari E, Gracia F, Khan MM, Mosquera E, Gupta VK. Conducting PANI stimulated ZnO system for visible light photocatalytic degradation of coloured dyes. J Mol Liq. 2016;221:1029–33.
[31] Dang G, Shi Y, Fu Z, Yang W. Polymer nanoparticles with dendrimer-Ag shell and its application in catalysis. Particuology. 2013;11(3):346–52.
[32] Subair R, Tripathi BP, Formanek P, Simon F, Uhlmann P, Stamm M. Polydopamine modified membranes with in situ synthesized gold nanoparticles for catalytic and environmental applications. Chem Eng J. 2016;295:358–69.
[33] Murugadoss A, Chattopadhyay A. A 'green' chitosan–silver nanoparticle composite as a heterogeneous as well as micro-heterogeneous catalyst. Nanotechnology. 2007;19(1):015603.